RSC Advances

This is an *Accepted Manuscript*, which has been through the Royal Society of Chemistry peer review process and has been accepted for publication.

Accepted Manuscripts are published online shortly after acceptance, before technical editing, formatting and proof reading. Using this free service, authors can make their results available to the community, in citable form, before we publish the edited article. This *Accepted Manuscript* will be replaced by the edited, formatted and paginated article as soon as this is available.

You can find more information about *Accepted Manuscripts* in the **Information for Authors**.

Surface platinum-rich CuPt bimetallic nanoparticles supported by partially unzipped vapor grown carbon fibers and their electrocatalytic activities

Han Mao, Lan Zhou, Tao Huang[*], Aishui Yu[*]

Department of Chemistry, Shanghai Key Laboratory of Molecular Catalysis and Innovative

Materials, Institute of New Energy, Fudan University, Shanghai 200438, China

Abstract

Here we prepare the CuPt/PUVGCF catalyst made of surface platinum-rich CuPt nanoparticles anchored on partially unzipped vapor grown carbon fibers (PUVGCFs) as an anode catalyst for fuel cells. Longitudinal unzipping of vapor grown carbon fibers (VGCFs) can get a combination structure of one-dimensional VGCF and two-dimensional graphene, inheriting good solubility and dispersity from VGCFs and big surface area from graphene, thus more integrated combination with CuPt nanoparticles. Electrochemical measurements show the CuPt/PUVGCF catalyst has superior catalytic activity and stability for methanol and ethanol electrooxidations compared to that of CuPt/VGCF, which may be a consequence of mutual effects of the CuPt bimetallic interaction and the excellent properties of PUVGCFs.

---

[*]Corresponding authors. Tel. & Fax: +86-21-51630320. *E-mail*: asyu@fudan.edu.cn (A. S. Yu);
Tel.: +86-21-51630321, Fax: +86-21-51630320. *E-mail*: huangt@fudan.edu.cn (T. Huang)

1. Introduction

Fuel cells, especially direct methanol fuel cells (DMFCs), are considered as highly promising future power sources due to their high-energy conversion efficiency, low pollutant emission, low operating temperature and economy [1,2]. Platinum is regarded as the most popular and effective anode catalyst component for methanol oxidation because of its superior catalytic activity and stability [3,4]. Although DMFCs are good alternative power sources, their properties needs to be improved in order to make them suitable for practical applications, the main problems need to be solved are the high cost and poor poison tolerance of Pt-based catalysts [5-7]. It is known that Pt itself suffers from CO poisoning during successive oxidation of methanol because the $(CO)_{ad}$ bonds tightly to the Pt atoms. To overcome this undesirable behavior, a common strategy is to alloy Pt with other hydrophilic elements which enable the $(CO)_{ad}$ to react with $(OH)_{ad}$ to form CO_2, thus the Pt surface can be recovered . Transition elements such as Ru, Ni, Pd, Rh, Mo, Au [8-15] are usually introduced to form binary or ternary alloys to enhance electrocatalytic performance. The application of noble metals makes it rather expensive, in view of this factor, we designed a structure in which the inexpensive copper acts as the core and a thin platinum layer as the catalytic shell. Literatures and previous work demonstrate that fabrication of the quasi core-shell structure and bimetallic effect do enhance the catalytic activity and stability [16-23].

2

Another important aspect is the support used to disperse the Pt phase. A good support

need certain features such as good electrical conductivity, good catalyst-support

interaction, large surface area, good water handling capability to avoid flooding, good

corrosion resistance, and easy recovery of the catalyst [24-27]. A good interaction

between the catalyst and the support not only improves catalyst efficiency and

decreases catalyst loss but also governs good charge transfer. Vapor-grown carbon

fibers (VGCFs) are commercial materials with a structure of hollow rods, produced by

depositing a layer of pyrocarbon from the vapor phase on a catalytically grown carbon

filament [28,29]. This morphology determines many properties of the fiber, since the

filament is more graphitic than the pyrocarbon. A similar carbonaceous material is

multiwalled carbon nanotubes (MWCNTs), but disadvantages of MWCNTs are their

poor dispersibility and expensiveness. Nevertheless, VGCFs exhibit good

dispersibility and similarly high electrical conductivity and high mechanical strength.

The price of VGCFs is also much lower than that of MWCNTs. One concern is that

the inner part of VGCFs will not be utilized, so we referred to the literature [30] and

used Hummers method to strip the outer layers of VGCFs to obtain the partially

unzipped vapor grown carbon fibers (PUVGCFs). PUVGCFs combine the structures

of one-dimensional tube and two-dimensional planar construction, which have a

graphene-like morphology with a broadened VGCF axis. PUVGCFs have much lager

specific surface area and is more stable after dispersing in solvents than pristine

VGCFs. Compared to pure graphene, PUVGCFs demonstrate better water solubility

and dispersity, which may be easier to handle as a support for fuel cell catalysts.

In this work, we developed a simple way to synthesize CuPt/PUVGCF catalyst. The cheapness of cupreous ingredient makes it a promising assistant for Pt-based catalysts. The CuPt/PUVGCF catalyst shows superior electrocatalytic activity and cycling stability compared to the referential CuPt/VGCF catalyst, showing that PUVGCFs are better anode catalyst supports for fuel cells.

2. Experimental Section

2.1 Catalyst preparation

The PUVGCFs were synthesized from VGCFs (provided by Showa Giken Industrial Co., Ltd, Japan) by the Hummers method according to the literature[31]. The pristine VGCFs (2 g) were put into cold (0 °C) concentrated H_2SO_4 (46 mL) solution containing 1 g $NaNO_3$. $KMnO_4$ (6 g) was added gradually with stirring and ice bath under 20 °C. Subsequently, the ice bath was removed and the flask was heated to 35 °C and maintained at this temperature for 30 min, followed by the slow addition of 92 mL of deionized water. The temperature of the reaction mixture was increased to 98 °C and the reaction vessel was maintained at this temperature for 15 min. Then, the suspension was further diluted with 280 mL of water and treated with 3% H_2O_2 until the cessation of gas evolution. Finally, the suspension was vacuum filtered and left to dry under vacuum overnight after washing with copious amounts of deionized water.

4

The CuPt nanoparticles were fabricated according to our previous work [18]. First, 120 mg (0.458 mmol) $Cu(acac)_2$ and 40 mg PVP_{K30} were dissolved in 80 ml ethylene glycol (EG) at 80 °C under N_2 atmosphere. The solution was ramped to 130 °C and aged for 3 hrs. After cooling down, 90mg (0.185mmol) K_2PtCl_6 was slowly added to the Cu/EG colloids at 80 °C under N_2 atmosphere, ramped to 110 °C and aged for 4hrs. CuPt NP colloidal suspension was diluted with acetone and centrifuged at 12000 rpm. The precipitates were washed with acetone-ethanol mixtures under sonication and then dispersed in ethanol. The obtained ethanol solution was divided equally into two parts, one mixed with 70mg VGCFs and the other mixed with 110mg PUVGCFs, respectively. The two mixtures were dried under the stirring, and the resulting catalysts were subjected to reduction in H_2/Ar at 250°C for 3 hrs. The obtained catalysts were denoted as CuPt/PUVGCF and CuPt/VGCF. The mass fraction of Pt is 9.8% for CuPt/PUVGCF and 9.1% for CuPt/VGCF . The ratio of Pt to Cu is about 1.76:1.

2.2 Material characterization

The as-prepared catalysts were characterized by X-ray diffraction (XRD) performed on a Bruker D8 Advance X-ray diffractometer using Cu Kα radiation with a *k* of 1.5406 Å at a scan rate of 4 deg min^{-1}. The catalyst morphologies were observed by transmission electron microscopy (TEM) (JEOL JEM-2010F UHR). The precise compositions were analyzed by Inductively Coupled Plasma (ICP).

2.3 Electrochemical measurement

The working electrodes for electrochemical experiments were prepared by thin film electrode method. A polished glassy carbon (GC, Φ 5 mm) was used as the substrate. Certain amount of sample was dispersed in 2.5 mL ethanol under sonication for ten minutes, and then 25 μL suspension was pipetted onto a GC substrate under sonication. After ethanol evaporation, the deposited catalysts were covered by 5 μL Nafion solution (0.5 wt%, Dupont). The typical platinum loading is equal, 4.5 ug Pt on each electrode. All electrochemical measurements were carried out on a CHI 660A electrochemical workstation (Shanghai Chenhua apparatus corporation, China) using a conventional three-electrode glassy cell with a platinum sheet and an Hg/Hg_2SO_4, K_2SO_4 electrode (MSE, 0.615 V vs. NHE) as the counter and reference electrodes.

3. Results and discussion

3.1 Physicochemical characterization

The morphologies and sizes of carbonaceous supports, catalysts and CuPt nanoparticles were characterized by TEM. As shown in Fig 1A, VGCFs are straight rods and around 150 nm in diameter, and up to several micron meters in length. Compared to the pristine VGCFs, the outside layers of PUVGCFs are longitudinally unzipped and present partially graphene-like morphology on the surface with a broadened VGCF axis (Fig 1B). The morphologies of CuPt/VGCF catalyst (Fig 1C) and CuPt/PUVGCF catalyst (Fig 1D) show that CuPt nanoparticles are well-dispersed

on both supports. Generally speaking, high dispersion of CuPt nanoparticles on the supports is essential to the electrocatalytic activity for methanol oxidation. Fig 1E and 1F show the HR-TEM image and HAADF-STEM image of CuPt nanoparticles, respectively. They both show the uniform nanostructure of CuPt with the sizes of 2-3 nm. The lattice is clearly observed, and the calculated d-spacing value is around 0.221 nm, compared to the standard 0.2265 nm of face centered cubic (fcc) Pt (1 1 1), the lattice is slightly contracted. This can be interpreted that the Pt lattice doped with minor radius Cu atoms sustains the lattice distortion and thus the contraction of interplanar spacing.

Fig 2 shows the XRD patterns of the as-prepared catalysts. The peaks around 26° in both curves are ascribed to the carbon support, and it's obvious that VGCFs are of good crystalline character while PUVGCFs get lower crystallinity due to their open edges and the formation of graphene-like structure. The diffraction peaks of CuPt/VGCF at around 42.8°, 53.8°, and 77.8° are attributed to the (100), (004), and (110) diffraction peaks of graphite [JCPDS: PDF 75-1621], respectively. The two catalysts have almost the same diffraction peaks observed at 40.6°, 47.3°, 69.4°, 83.6° , indexed as the (111), (200), (220), (311) planes of a face centered cubic (fcc) structure. These peaks can neither match the Pt phase nor the Cu phase well, whereas the peaks are more close to the Pt phase rather than Cu phase. Considering Cu and Pt both belong to Fm-3m (225) space groups and Pt and Cu can form solid solution, the XRD patterns stand good chance of incorporation of Cu into the Pt lattice, instead of

the reverse manner. Because of the Kirkendall effect [32], the inner Cu atoms will enter the Pt lattice, thus the Pt lattice contracts and the peaks integrally shift to the high angles.

In order to investigate the oxidation states and surface composition of CuPt nanocomposites, X-ray photoelectron spectroscopy (XPS) analyses were performed (Fig 3A and 3B). The detectable depth of XPS is about 2-10 nm, larger than the diameter of CuPt nanoparticles, however, the surface Pt/Cu atomic ratio (2.0:1) is larger than the bulk composition ratio (1.76:1), which is a side proof of the surface platinum rich structure. In Fig 3B, the asymmetric peaks with a doublet centered at 71.0 and 74.4 eV, respectively, are mainly ascribed to Pt^0 4f 7/2 and Pt^0 4f 5/2. There also exist little platinum oxidation states (Pt^{2+}) in the nanocomposites due to the long time contact with air.

Raman spectroscopy (Figure 3C) was applied to investigate the different properties between VGCFs and PUVGCFs. For carbon materials, the G-band is common to all sp^2 carbon forms, and the D-band arosed from phonon branches is significant in providing information about the electronic and geometrical structures from defects. The intensity ratio of the D and G bands (I_D/I_G) is commonly used to measure the disorder and crystallite size of carbon materials [33,34]. Negligible D-band is observed for VGCFs, suggesting the high quality of the starting materials. As for

PUVGCFs, the prominent D-band at 1358 cm^{-1} and G-band at 1590 cm^{-1} are characterized. The I_D/I_G for PUVGCFs is much bigger than that for VGCFs, considering that defect density on the pristine VGCFs is low, the D-band Raman signal of our PUVGCFs should be mainly due to their open edges and the formation of graphene-like structure. The specific Brunauer-Emmett-Teller (BET) tests of VGCFs and PUVGCFs (Fig 3D) back the Raman results. Due to the formation of graphene-like structure, the BET surface area of VGCFs arises from 11 m^2 g^{-1} to around 190m^2 g^{-1} after the longitudinal unzipping.

3.2 Electrochemical Characterization

The electrochemical characterizations of CuPt/PUVGCF catalyst were investigated, and the CuPt/VGCF catalyst was also researched for comparison. To evaluate the geometric structure of the Pt surfaces, cyclic voltammetry (CV) experiments were conducted in 0.5 M H$_2$SO$_4$ solution (Fig 4A). The multiple peaks between -0.65 V to -0.37 V (vs. MSE) are attributed to the adsorption/desorption of hydrogen and can be used to calculate the electrochemical active surface area (ECSA). The calculated ECSAs are 37.2 m^2 g^{-1} and 47.4 m^2 g^{-1} for CuPt/VGCF and CuPt/PUVGCF, respectively. The broadened CV curve of CuPt/PUVGCF indicates the larger specific surface area of the carbon support, which is in accordance with the above characterizations.

The catalytic activity of methanol oxidations on the two catalysts were measured by cyclic voltammetry in a solution of 0.5 M H_2SO_4 and 0.5 M CH_3OH. The catalytic activity was evaluated as Pt mass specific current. Both CV curves (Fig 4B) show a similar forward anodic peak current of methanol oxidation and and a reverse anodic peak current. The forward anodic peak current density is about 780 mA mg^{-1} Pt for CuPt/PUVGCF composite and 500 mA mg^{-1} Pt for CuPt/VGCF. The forward anodic peak current density for CuPt/PUVGCF is about 1.5 times that for CuPt/VGCF, in accord with the ECSA results. Besides, the potential of forward anodic peak for CuPt/PUVGCF shifts about 0.05V negatively than that for CuPt/VGCF, signifying easier methanol oxidation at the CuPt/PUVGCF electrode. The high electrocatalytic activity of CuPt/PUVGCF may root in the mutual effects of quasi core-shell structure of CuPt nanoparticles and the outstanding inherent properties of PUVGCFs. It is supposed that PUVGCFs enhance charge transfer and the combination between the CuPt nanoparticles and the carbon support, thus improve catalyst efficiency and decrease catalyst loss.

Fig 4C displays the results of stability test of multicycle CV experiments for the two catalysts. The curves show the variation of forward anodic peak current density with the cycle number. There's an apparent trend of current decay for CuPt/VGCF as the CV cycles increase, the peak current declines rapidly and retains less than 50% after 1500 cycles. But CuPt/PUVGCF catalyst can maintain about 55% current density after 3500 cycles. The longitudinal zipping of VGCFs significantly enhances the

stability and durability of the catalyst, the reason may be the enlarged specific surface

area of PUVGCFs lead to the better dispersity of CuPt nanoparticles, and the 2-D

planar structure may have more tight effect with metal particles, and the CuPt

nanoparticles are more stable and not easy to grind down. Besides, the residual

oxygen-functional groups on PUVGCFs may also help to enhance the tolerance

toward CO for the catalysts [35].

To confirm the long-term durability of CuPt/PUVGCF and CuPt/VGCF catalysts

toward methanol oxidation, chronoamperometry experiments were performed for a

duration of 1000 s. Fig 4D shows the current - time curves for the two catalysts, both

electrodes display a current decay during the initial period because of the formation of

intermediate species such as CH_3OH_{ads} and CHO_{ads}. The long time decay has been

attributed to the adsorbed SO_4^{2-} anions on the catalyst surface, which tend to inhibit

the oxidation of methanol. The current density for CuPt/PUVGCF catalyst keeps

higher than that for CuPt/VGCF throughout the test range, and the rate of current

decay is slower for CuPt/PUVGCF, indicating that CuPt/PUVGCF have the superior

catalytic stability for methanol oxidation. This result is in agreement with the

behaviors in the cyclic voltammetry experiments, which can be attributed not only to

the synergistic effects of the quasi core-shell bimetallic components, but also to the

good preservation of the intrinsically electronic conductivity of PUVGCFs.

Moreover, we conducted the chronopotentiometry experiments to study the poison resistance of catalysts for methanol oxidation. In this experiment, the potential must increase to fulfill the applied current until a potential is reached where larger amounts of H_2O can be decomposed due to excessive coverage of residues. Fig. 4E shows the chronopotentiometry curves for CuPt/VGCF and CuPt/PUVGCF catalysts. The chronopotentiometry curve displays a trend that electrode potential increases gradually for a certain time and then suddenly jumps to a much higher potential. The time at which the electrode potential jumps to a higher potential can be used to judge the antipoisoning ability of catalysts. As can be seen, CuPt/VGCF catalyst needs about 0.1V and only maintains 20s. Comparatively, CuPt/PUVGCF catalyst needs 1600s to jump to the higher potential. The results further prove that CuPt/PUVGCF has the better electrocatalytic property and poison resistance.

Since the catalyst behaves well in methanol oxidation, we tried the ethanol oxidation. Although direct ethanol fuel cells receive much attention since ethanol is environmentally friendly, easy to be produced in large quantities, and has a high energy density, the severe situation is the sluggish kinetics and low activity on platinum-based catalysts [36]. In this article, ethanol oxidation is carried out in a solution of 0.5 M H_2SO_4 and 0.5 M C_2H_5OH. Both CV curves (Fig 5) show well-separated anodic peaks in the forward and reverse scans, similar to that of the methanol oxidation reaction in acid media. The reverse peak current density for ethanol oxidation on CuPt/PUVGCF electrode is 230 mA mg^{-1} Pt, much higher than

140 mA mg^{-1} Pt on CuPt/VGCF electrode. However, compared to methanol oxidation, it's obvious that the current densities for ethanol oxidation are much lower. This may be the complex and tardy kinetics of ethanol oxidation. In this part, more incisive research need to be done.

4. Conclusions

In conclusion, we synthesized a novel surface platinum-rich CuPt/PUVGCF catalyst for methanol and ethanol electrooxidations by an easy method. PUVGCFs have a combination of one-dimension and two-dimension structure, thus inheriting the dispersity and solubility from VGCFs and big surface area from graphene. The mutual functions of bimetallic structure and tighter interaction between metal particles and PUVGCFs result in preponderant catalytic activity, especially in stability, durability and poison tolerence in electrochemical experiments, which are difficult to overcome for fuel cell anode catalysts. The synergistic properties within CuPt bimetallic compounds and the mutual effects between metal particles and PUVGCFs still ask for more work.

Acknowledgments

References

[1] A. S. Aricò, S. Srinivasan and V. Antonucci, *Fuel Cells,* 2001, **1,** 133-161.

[2] L. Dong, R. R. S. Gari, Z. Li, M. M. Craig and S. Hou, *Carbon,* 2010, **48,** 781-787.

[3] H. S. Liu, C. J. Song, L. Zhang, J. J. Zhang, H. J. Wang and D. P. Wilkinson, *J. Power Sources,* 2006, **155,** 95-110.

[4] E. Antolini, *Mater. Chem. Phys.,* 2003, **78,** 563-573.

[5] W. Zhou, Z. Zhou, S. Song, W. Li, G. Sun, P. Tsiakaras and Q. Xin, *Appl. Catal. B: Environ.,* 2003, **46,** 273-285.

[6] J. Yang, J. Y. Lee, Q. Zhang, W. Zhou and Z. Liu, *J. Electrochem. Soc.,* 2008, **155,** B776-B781.

[7] T. Takeguchi, T. Yamanaka, K. Asakura, E. N. Muhamad, K. Uosaki and W. Ueda, *J. Am. Chem. Soc.,*, 2012, **134**, 14508-14512.

[8] G.-R. Zhang, D. Zhao, Y.-Y. Feng, B. Zhang, D. S. Su, G. Liu and B.-Q. Xu, *ACS Nano,* 2012, **6,** 2226-2236.

[9] B. Singh, L. Murad, F. Laffir, C. Dickinson and E. Dempsey, *Nanoscale,* 2011, **3,** 3334-3349.

[10] N. S. Porter, H. Wu, Z. Quan and J. Fang, *Acc. Chem. Res.*, 2013, **46**, 1867-1877.

[11] S.-S. Li, J.-J. Lv, Y.-Y. Hu, J.-N. Zheng, J.-R. Chen, A.-J. Wang and J.-J. Feng, *J. Power Sources,* 2014, **247,** 213-218.

[12] Y. Wei, Z. Zhao, T. Li, J. Liu, A. Duan and G. Jiang, *Appl. Catal. B: Environ.,* 2014, **146,** 57-70.

[13] Y. Hu, P. Wu, H. Zhang and C. Cai, *Electrochim. Acta,* 2012, **85,** 314-321.

[14] Z.-F. Xu and Y. Wang, *J. Phys. Chem. C,* 2011, **115,** 20565-20571.

[15] E. Lee, A. Murthy and A. Manthiram, *Electrochim. Acta,* 2011, **56,** 1611-1618.

[16] X. Ge, L. Chen, J. Kang, T. Fujita, A. Hirata, W. Zhang, J. Jiang and M. Chen, *Adv. Funct. Mater.,* 2013, **23,** 4156-4162.

[17] Y. Kang, J. B. Pyo, X. Ye, R. E. Diaz, T. R. Gordon, E. A. Stach and C. B. Murray, *ACS Nano*, 2012, **7,** 645-653.

[18] H. Mao, R. Li, K. Jiang, T. Huang and A. Yu, *Electrochim. Acta,* 2013, **107,** 419-424.

[19] S. Chen, Z. Wei, X. Qi, L. Dong, Y.-G. Guo, L. Wan, Z. Shao and L. Li, *J. Am. Chem. Soc.,*, 2012, **134**, 13252-13255.

[20] C. Galeano, J. C. Meier, V. Peinecke, H. Bongard, I. Katsounaros, A. A. Topalov, A. Lu, K. J. J. Mayrhofer and F. Schüth, *J. Am. Chem. Soc.,*, 2012, **134**, 20457-20465.

[21] Z. Wen, Q. Wang and J. Li, *Adv. Funct. Mater.,* 2008, **18,** 959-964.

[22] S. Alayoglu, P. Zavalij, B. Eichhorn, Q. Wang, A. I. Frenkel and P. Chupas, *ACS Nano,* 2009, **3,** 3127-3137.

[23] Q. Yuan, D. Duan, Y. Ma, G. Wei, Z. Zhang, X. Hao and S. Liu, *J. Power Sources,* 2014, **245,** 886-891.

[24] R. E. Rettew, N. K. Allam and F. M. Alamgir, *ACS Appl. Mat. Interfaces,* 2011, **3,** 147-151.

[25] A. Mondal and N. R. Jana, *ACS Catal.,* 2014, 593-599.

[26] Z. Li, X. Huang, X. Zhang, L. Zhang and S. Lin, *J. Mater. Chem.,* 2012, **22,** 23602-23607.

[27] Y. M. Volfkovich, V. E. Sosenkin and V. S. Bagotsky, *J. Power Sources,* 2010, **195,** 5429-5441.

[28] Y. K. Choi, K. Sugimoto, S. M. Song, Y. Gotoh, Y. Ohkoshi and M. Endo, *Carbon,* 2005, **43,** 2199-2208.

[29] Z. Guo, J. Wang, F. Wang, D. Zhou, Y. Xia and Y. Wang, *Adv. Funct. Mater.,* 2013, **23,** 4840-4846.

[30] L. Jiao, L. Zhang, X. Wang, G. Diankov and H. Dai, *Nature,* 2009, **458,** 877-880.

[31] W. S. Hummers and R. E. Offeman, *J. Am. Chem. Soc.,* 1958, **80,** 1339-1339.

[32] J. X. Wang, C. Ma, Y. Choi, D. Su, Y. Zhu, P. Liu, R. Si, M. B. Vukmirovic, Y. Zhang and R. R. Adzic, *J. Am. Chem. Soc.,* 2011, **133,** 13551-13557.

[33] A. C. Ferrari, *Solid State Commun.,* 2007, **143,** 47-57.

[34] M. S. Dresselhaus, A. Jorio, M. Hofmann, G. Dresselhaus and R. Saito, *Nano Lett.,* 2010, **10,** 751-758.

[35] W. He, H. Jiang, Y. Zhou, S. Yang, X. Xue, Z. Zou, X. Zhang, D. L. Akins and H. Yang, *Carbon,* 2012, **50,** 265-274.

[36] S. Guo, S. Dong and E. Wang, *Energy Environ. Sci.,* 2010, **3,** 1307-1310.

Figure Captions

Fig 1. TEM images of (A) VGCFs, (B) PUVGCFs, (C) CuPt/VGCF, (D) CuPt/PUVGCF, (E) HR-TEM image of CuPt nanoparticles, (F) HAADF-STEM image of CuPt nanoparticles.

Fig 2. XRD patterns of (i) CuPt/VGCF and (ii) CuPt/PUVGCF, the green vertical lines representing the standard (fcc) Pt phase,and the blue for (fcc) Cu.

Fig 3. XPS pattern of (A) CuPt/PUVGCF and (B) Pt 4f spectra; (C) Raman spectra, (D) BET diagram. In all images, i stand for CuPt/VGCF and ii for CuPt/PUVGCF.

Fig 4. (A) CV curves in 0.5 M H_2SO_4 solution at a scan rate of 50 mV s^{-1}.(B) Methanol electrooxidation curves and (C) The scatter diagram of peak current density varied with cycle number in a solution of 0.5 M CH_3OH and 0.5 M H_2SO_4 at a scan rate of 50 mV s^{-1} . (D) Chronoamperometry curves polarizing at 0.2 V. (E) Chronopotentiometry curves with an anodic current of 1 mA. In all images, i for CuPt/VGCF and ii for CuPt/PUVGCF.

Fig 5. Ethanol oxidation curves in 0.5 M H_2SO_4 and 0.5 M C_2H_5OH solution at a scan rate of 50 mV s^{-1}, i for CuPt/VGCF and ii for CuPt/PUVGCF.
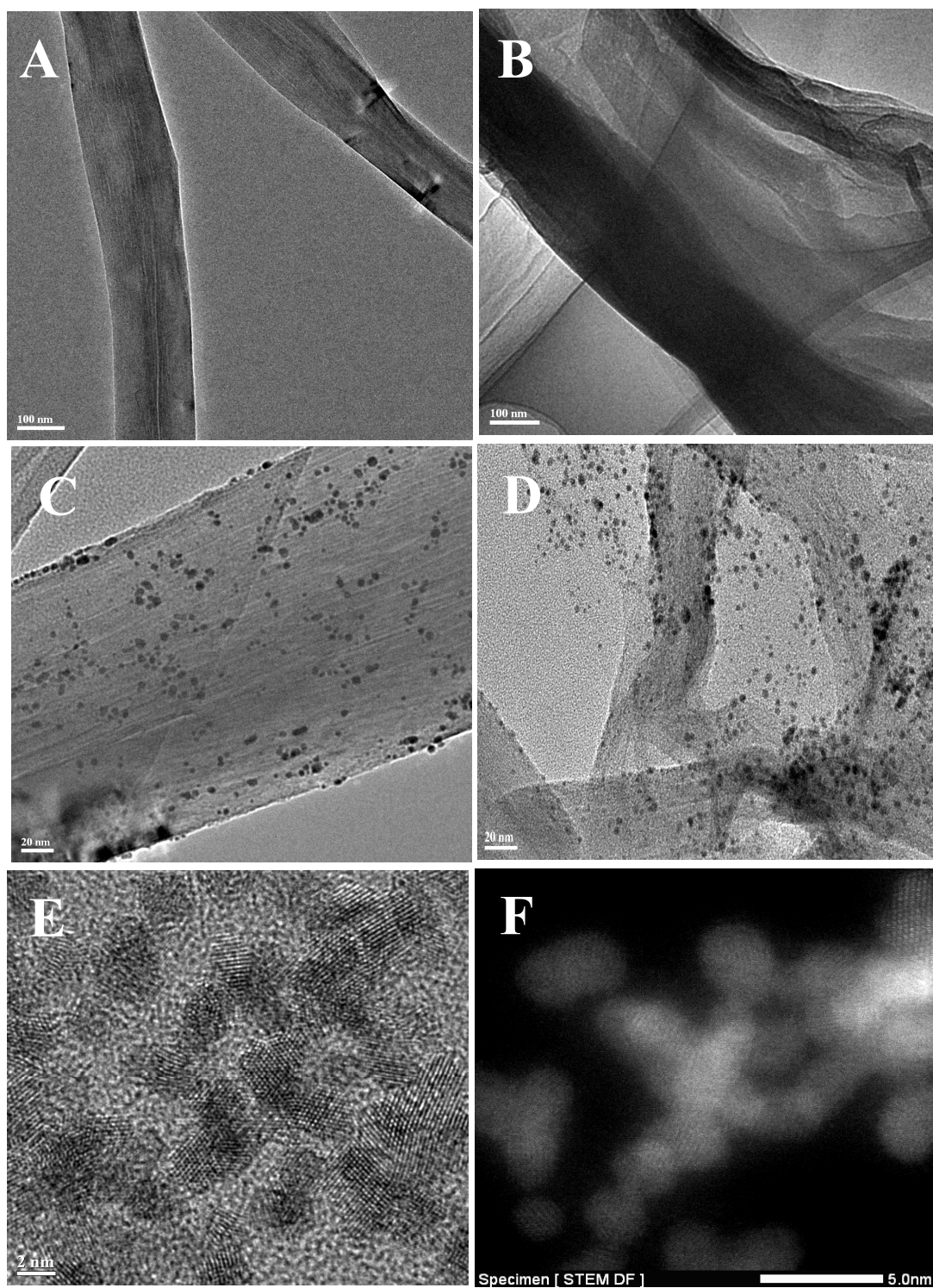
Fig 1. TEM images of (A) VGCFs, (B) PUVGCFs, (C) CuPt/VGCF, (D) CuPt/PUVGCF, (E) HR-TEM image of CuPt nanoparticles, (F) HAADF-STEM image of CuPt nanoparticles.
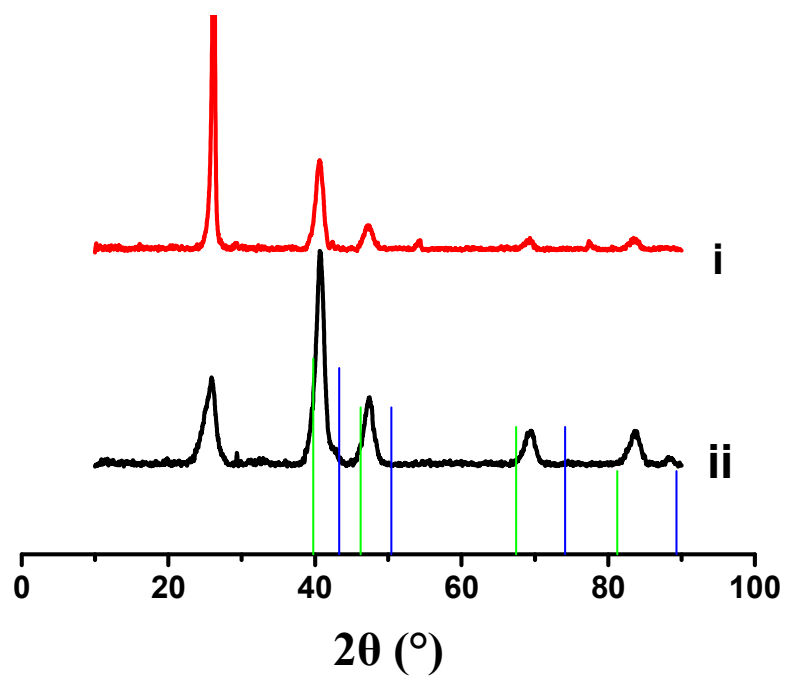
Fig 2. XRD patterns of (i) CuPt/VGCF and (ii) CuPt/PUVGCF, the green vertical

lines representing the standard (fcc) Pt phase,and the blue for (fcc) Cu.
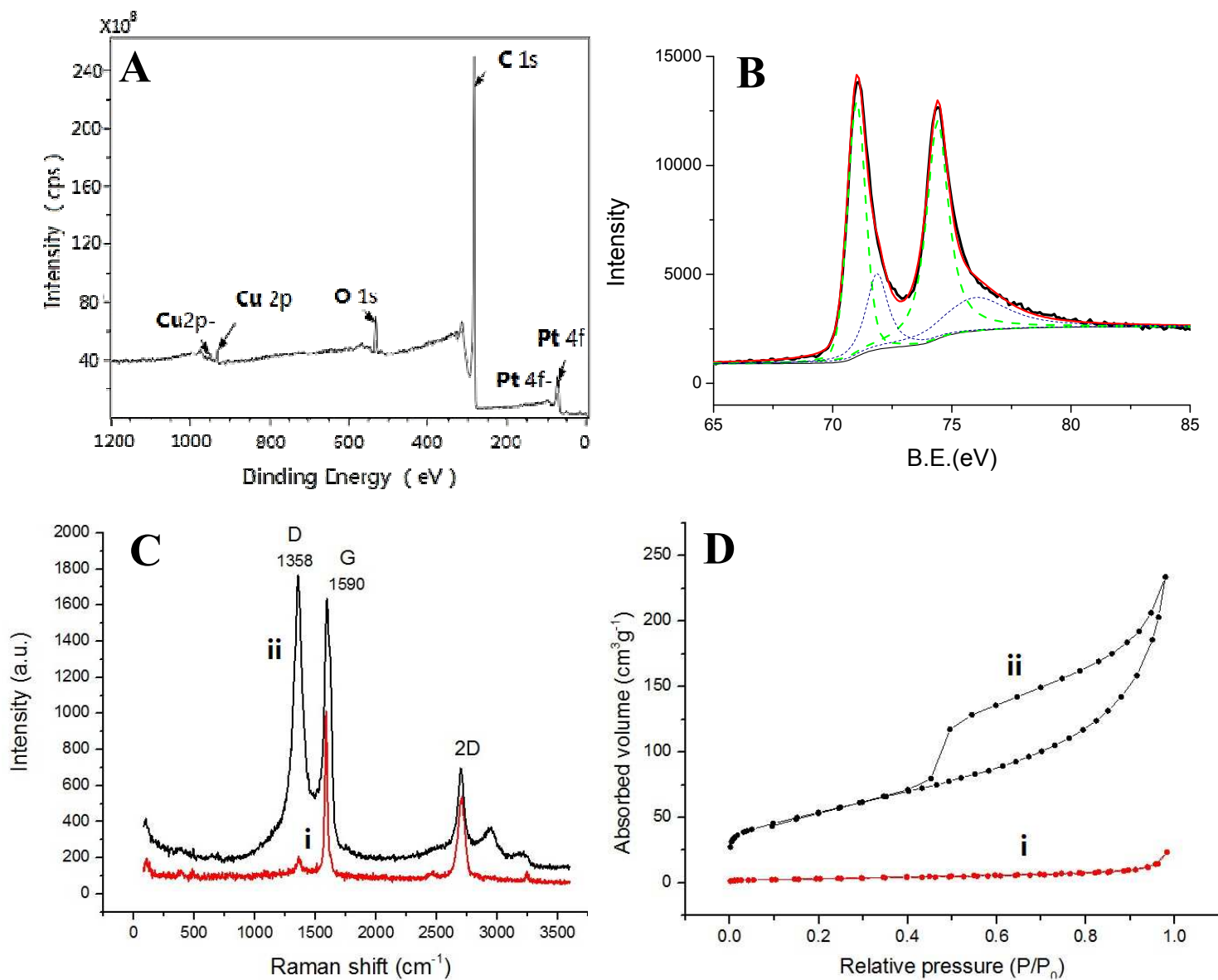
Fig 3. XPS patterns of (A) CuPt/PUVGCF and (B) Pt 4f spectra; (C) Raman spectra,

(D) BET diagram. In all images, i stand for CuPt/VGCF and ii for CuPt/PUVGCF.

RSC Advances
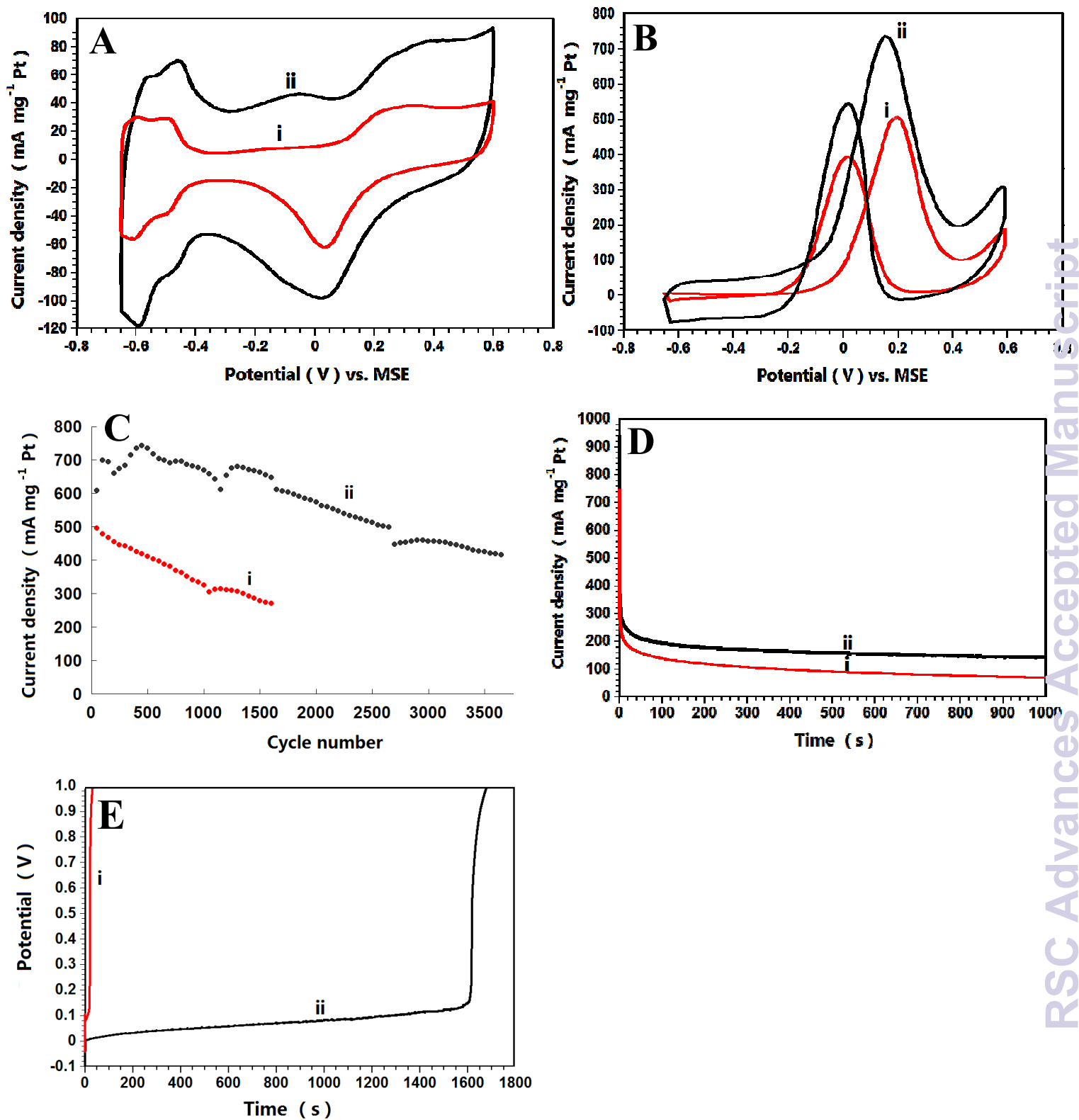
Fig 4. (A) CV curves in 0.5 M H₂SO₄ solution at a scan rate of 50 mV s⁻¹.(B) Methanol electrooxidation curves and (C) The scatter diagram of peak current density varied with the cycle number in a solution of 0.5 M CH₃OH and 0.5 M H₂SO₄ at a scan rate of 50 mV s⁻¹ . (D) Chronoamperometry curves polarizing at 0.2 V. (E) Chronopotentiometry curves with an anodic current of 1 mA. In all images, i for CuPt/VGCF and ii for CuPt/PUVGCF.

Fig 5. Ethanol oxidation curves in 0.5 M H₂SO₄ and 0.5 M C₂H₅OH solution at a scan rate of 50 mV s⁻¹, i for CuPt/VGCF and ii for CuPt/PUVGCF.